Determination of Opening Mode Stress Intensity Factor for Edge Cracks by Means of Digital Shearography Including Analytical and Numerical Simulations

A. Ghazavizadeh and N. Soltani
Mech. Eng. Department, Tehran Univ.

B. Hakimelahi and M. Ghasemieh
Civil. Eng. Department, Tehran Univ.

ABSTRACT

In this paper, opening mode stress intensity factor (SIF) for edge cracks has been obtained by means of non-destructive optical technique of digital shearography. The resulting fringes were simulated by both analytical relations and finite element method (FEM). Then shearographic relations and linear elastic fracture mechanics relations were incorporated to develop an algorithm to determine K_I. To utilize the advantage of "whole field" shearography and to minimize random experimental errors, the least squares method is used to obtain SIF. The comparison of fringes, as well as shearography and empirical K_I values, shows good agreements between simulation and experimental results and proves the credibility of experimental fringes and potentials of this non-destructive method in measurement applications.

Key Words: Digital Shearography, Finite Element Method, Stress Intensity Factor

تعیین ضریب شدت تنش مود بازشوندگی در ترک‌های لبه‌ای با استفاده از برشنگاری دیجیتالی به همراه شبیه‌سازی‌های عددی و تحلیلی

اکبر قضاوی‌زاده[1] و ناصر سلطانی[2]
دانشکدهٔ مهندسی مکانیک، دانشگاه تهران

بهزاد حکیم‌الهی[3] و مهدی قاسمیه[4]
دانشکدهٔ مهندسی عمران، دانشگاه تهران

چکیده

در مقالهٔ حاضر ضریب شدت تنش مود بازشوندگی در ترک‌های لبه‌ای با استفاده از تکنیک نوری غیر مخرب برشنگاری دیجیتالی تعیین گردیده و هاله‌های به‌دست آمده با استفاده از روابط تحلیلی و روش اجزاء محدود شبیه‌سازی شده‌اند. روابط برشنگاری و نیز روابط مکانیک شکست الاستیک خطی با یکدیگر ترکیب شده‌اند تا الگوریتمی برای تعیین ضریب شدت تنش (K_I) به‌دست آید. به منظور بهره‌گیری از ویژگی میدانی برشنگاری و همچنین به حداقل رساندن خطای داده‌های تجربی، برای بدست آوردن ضریب شدت تنش مورد نظر از روش حداقل مربعات استفاده شده‌است. مقایسهٔ هاله‌های شبیه‌سازی شده و مقادیر تجربی و تئوری ضریب شدت تنش نشان دهندهٔ میزان اعتبار این تکنیک و توانایی‌های آن در مسائل کاربردی می‌باشد.

واژه‌های کلیدی: برشنگاری دیجیتالی، اجزاء محدود، ضریب شدت تنش.

۱- کارشناس ارشد: akbar_ut@yahoo.com
۲- دانشیار: nsoltani@ut.ac.ir
۳- دانشجوی دکتری: bhakim@ut.ac.ir
۴- استادیار: mghassem@ut.ac.ir

1. Introduction

Digital shearography is a relatively new non-destructive evaluation technique developed to eliminate some of the shortcomings of holography. This technique which was introduced in the early 80's, has received a great deal of attention on the part of industrial and research centers [1-9]. In holography or Speckle Pattern Interferometry (SPI), surface displacements are measured while shearography measures surface displacement derivatives directly [10-12] and to obtain strain information, no numerical differentiation from displacement data is required. Moreover it eliminates the need for the reference beam in holography or SPI, thus making the optical setup simple and not requiring of any special vibration isolation device. The main advantage of shearography over other optical techniques is that environmental stability during testing need not to be stringently enforced. With these advantages, shearography has offered itself as a viable and efficient NDT tool in the industrial environments. Some potential applications for using laser diode shearography as an NDE tool are: on aircraft inspection, process control, quality control, bridge inspection, and NDT service companies.

Shearography is equivalent to a full field strain gage; it reveals defects by looking for defect-induced strain anomalies. This approach is superior to other techniques in that it allows defects criticality to be qualified. Moreover it is a fast non-contacting, and full field method.

There are two well known types of shearography: 1) Photographic shearography which is traditional one and 2) Digital shearography. The optical theory is the same for the digital and the photographic shearography, but technically digital shearography is a computerized When the light reflects from the surface of the object, it is focused on the image plane process which eliminates wet processing and reconstruction. The former uses photographic film as the recording medium which is slow and costly. Furthermore, a subsequent Fourier filtering process is needed for the readout of fringe patterns [14, 15] which further delays the output of the test results. Instead the latter employs a computerized process which is more user friendly and cost efficient. It uses a CCD-camera as the recording medium and digital processing to obtain image data and analyze the results. This leads to rapidly increased testing speed so that the shearogram can be observed in real time (i.e. at video rate). One drawback of shearography is that due to the limited resolution of today's video cameras and frame image digitizers, the quality of the fringe patterns are poor.

In the present work shearography was used for determination of first mode SIF in edge cracked specimens and the resulting fringe shapes were simulated both by FEM and by analytical relations, derived by merging the mathematical relations of linear elastic fracture mechanics and optical relations. Since all the known finite element packages do not deliver contours of out-of-plane displacement derivatives directly, in FEM simulation part, programming has been done to display the desired contours.

2. Principles of Shearography

A typical experimental optical setup of digital shearography is shown in Fig. 1. The test object is illuminated by an expanded laser beam. The light reflected from the object surface is focused on the image plane of an image shearing CCD-camera where a shearing device (Michelson interferometer) is implemented in front of it's lens. The Michelson interferometer consists of a beam splitter and two orthogonally placed mirrors on two sides of the beam splitte of the CCD-camera via these two mirrors [14]. By turning mirror 1 for a very small

angle from the normal position, a pair of laterally sheared images of the test object is generated on the CCD-camera. The two sheared images interfere with each other producing a speckle pattern (Fig. 1). Since contrary to SPI this technique does not require separate object and reference beams, it is called a "self-referencing" technique.

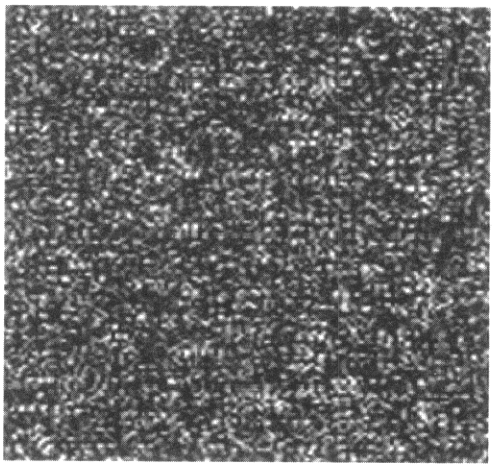

Fig.1. A typical speckle pattern.

The intensity distribution I(x, y) of the speckle pattern is given by:

$$I(x, y) = I_0[1+\gamma \cos(\varphi(x, y))], \quad (1)$$

where, I_0 represents the average intensity of these two sheared light waves, γ represents the modulation of the interference term and $\varphi(x, y)$ represents the random relative phase angle between the two sheared images before the object is deformed. This intensity distribution is registered by the CCD-camera and is processed by using a computer. When the object is deformed the intensity distribution of the speckle pattern is slightly altered, represented as:

$$I'(x, y) = I_0[1+\gamma \cos(\varphi'(x, y))]. \quad (2)$$

It is recorded by the CCD-camera again and saved on the computer. Digital subtraction of Eq.(1) and Eq.(2) yields:

$$I_s = I - I' = I_0[\gamma \cos\varphi - \gamma \cos(\varphi+\Delta)]$$
$$= 2I_0\gamma \sin(\varphi+\frac{\Delta}{2}) \sin(\frac{\Delta}{2}) \quad (3)$$

The result of the subtraction operation between the two digitized information yields a fringe pattern, i.e. the so called 'digital shearogram', which describes the relative phase change Δ $[\Delta = \varphi'(x, y) - \varphi(x, y)]$ due to the object deformation, and it is displayed on the monitor in real time (at video rate).

From Eq. (3) it is concluded that if $\Delta=2\pi N$, where N is an integer, dark fringes are formed. In this way dark fringes can be sequentially numbered with integers. The procedure of assigning fringes with numbers is similar to other optical methods and is done manually along with the analysis of fringes.

It can be shown that the relative phase change is related to the displacement derivatives instead of displacement itself due to the shearing function of shearography. If the shearing direction is in the x direction, Δ is given by:

$$\Delta_x = (\frac{\partial u}{\partial x}\vec{k}_s.\vec{e}_x + \frac{\partial v}{\partial x}\vec{k}_s.\vec{e}_y + \frac{\partial w}{\partial x}\vec{k}_s.\vec{e}_z)\delta_x, \quad (4)$$

where, $\vec{k}_s$ is sensitivity vector; δ_x the amount of image shearing that is directed along the reference x- axis; $\vec{e}_x$, $\vec{e}_y$ and $\vec{e}_z$ unit vectors in x, y, z direction respectively and u, v, w the displacement components along the reference x- , y- , z- axis respectively. In the case where the shearing direction lies in the y direction, Eq. (4) becomes:

$$\Delta_y = (\frac{\partial u}{\partial y}\vec{k}_s.\vec{e}_x + \frac{\partial v}{\partial y}\vec{k}_s.\vec{e}_y + \frac{\partial w}{\partial y}\vec{k}_s.\vec{e}_z)\delta_y. \quad (5)$$

It has been shown [11] that the sensitivity vector has the magnitude $|\vec{k}_s| = 4\pi/\lambda \cos(\beta/2)$, where λ is illuminating light wavelength and β is the angle between illuminating and viewing direction, and lies along the bisector of the angle β (Fig. 2).

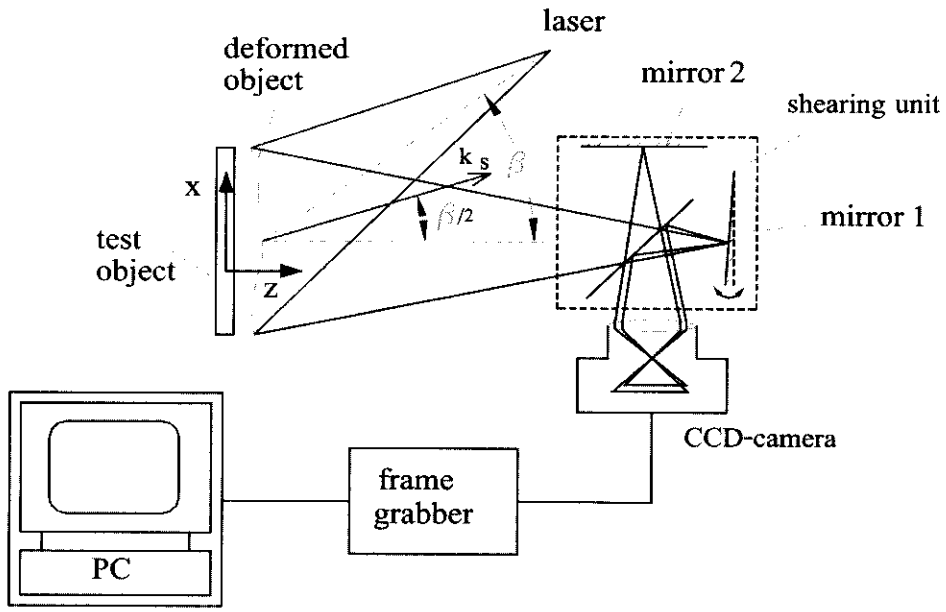

Fig. 1. A typical experimental setup of digital shearography.

If the illuminating angle β is normal to the object, the sensitivity vector $\vec{k}_s$ lies exactly in the z direction. In this case, because $\vec{k}_s . \vec{e}_x = \vec{k}_s . \vec{e}_y = 0$ and $\vec{k}_s . \vec{e}_z = |\vec{k}_s|$, Eqs. (4) and (5) reduce to:

$$\Delta_x = \frac{\partial w}{\partial x}|\vec{k}_s|\delta_x , \quad (6)$$

$$\Delta_y = \frac{\partial w}{\partial y}|\vec{k}_s|\delta_y , \quad (7)$$

where, $|\vec{k}_s|$, δ_x and δ_y are known system parameters and Δ can be obtained by using the conventional technique of finding the fringe orders. Hence the out of plane components $\partial w/\partial x$ or $\partial w/\partial y$ can be measured.

3. Experiment Procedure

The experiments include six test cases that were run by two specimens under different loads (Table 1).

Table 1. Associated specimen and loading of the test cases.

Case	Specimen No.	Loading (N)
1	1	227.6
2	1	433.6
3	1	528.8
4	2	209.9
5	2	334.5
6	2	508.2

The scheme and geometrical specifications of the specimens are detailed in Fig. 3 and Table 2. Making $L/W > 4$ creates uniform tension in the specimens which were machined out of a 3mm thick Plexiglas sheet. Young's modulus of elasticity and Poisson's ratio of the specimens material are 3.34 (GPa) and 0.33, respectively. The wavelength of the employed He-Ne laser is 632.8 (nm). In all test cases the amount of shear was 1 mm (in this example δ_y = 1 mm). The speckle pattern images taken by the digital camera were recorded and saved on

a computer. Subtracting before and after loading images, the fringes demonstrating $\partial w/\partial y$ appear. For typical cases 2, 3 and 6, experimental shearographic fringes are demonstrated in Fig. 4(a-c).

4. Analytical Simulation of Fringes

The out of plane component of displacement in plane stress mode is represented as:

$$w(r,\theta) = -\frac{\upsilon h}{2E}\left(\sigma_x(r,\theta) + \sigma_y(r,\theta)\right), \qquad (8)$$

where, υ, h and E represent Poisson's ratio, specimen thickness and Young's modulus of elasticity, respectively.

According to linear elastic fracture mechanics relations, near crack tip stresses σ_x and σ_y are (e.g. [17]):

$$\sigma_x(r,\theta) = \frac{K_I}{\sqrt{2\pi r}}\cos\frac{\theta}{2}\left(1 - \sin\frac{\theta}{2}\sin\frac{3\theta}{2}\right), \qquad (9)$$

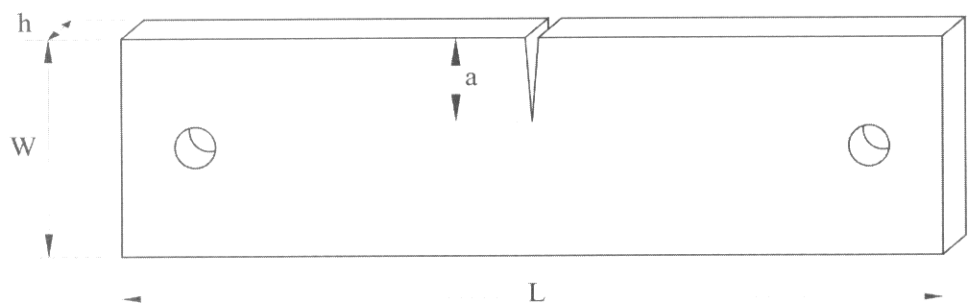

Fig.3. Scheme of the specimens.

Table 2. Geometric specifications of specimens.

Specimen No.	Width, W (mm)	Crack length, a (mm)	$\frac{a}{W}$	Thickness, h (mm)	Length, L (mm)
1	56.5	11.1	0.195	3	257
2	56.5	16.6	0.291	3	257

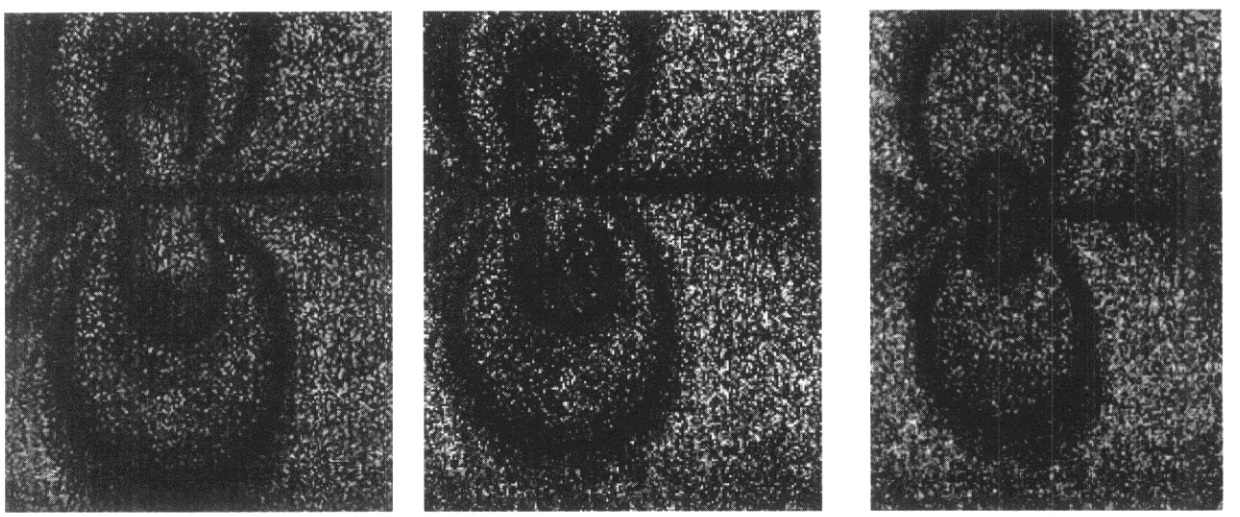

Fig. 4. Shearographic fringes; (a) case 2, (b) case 3, (c) case 6.

$$\sigma_y(r,\theta)=\frac{K_I}{\sqrt{2\pi r}}\cos\frac{\theta}{2}\left(1+\sin\frac{\theta}{2}\sin\frac{3\theta}{2}\right), \quad (10)$$

where, the origin of the polar coordinates is taken at the crack tip (Fig. 5). Substituting Eqs. (9) and (10) into Eq. (8), w is rewritten as:

$$w(r,\theta)=-\frac{\upsilon h K_I}{E\sqrt{2\pi r}}\cos\frac{\theta}{2}. \quad (11)$$

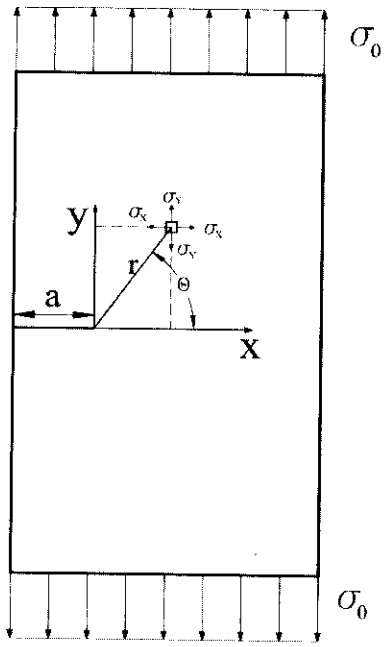

Fig. 5. Schematic illustration of relative position of applied coordinate systems.

Through transforming partial differential relations from polar coordinates into Cartesian coordinates, first partial derivative components of displacement will become:

$$\frac{\partial w}{\partial x}=\frac{\upsilon h K_I}{2Er\sqrt{2\pi r}}\cos\frac{3\theta}{2}, \quad (12)$$

$$\frac{\partial w}{\partial y}=\frac{\upsilon h K_I}{2Er\sqrt{2\pi r}}\sin\frac{3\theta}{2}. \quad (13)$$

In order to predetermine or in other words simulate fringe shapes, a polar relation containing K_I and N is sought. Right hand side of Eqs. (12) or (13) can be substituted into Eqs. (6) or (7) respectively. For instance by substituting Eq. (13) into Eq. (7), it follows:

$$\Delta_y=\frac{2\pi\upsilon h K_I\delta_y}{\lambda Er\sqrt{2\pi r}}\sin\frac{3\theta}{2}. \quad (14)$$

On the other hand for dark fringes, $\Delta_y = 2\pi N_y$ where N_y is an integer number. Accordingly:

$$\frac{1}{r\sqrt{r}}\sin\frac{3\theta}{2}=\frac{N_y\lambda E\sqrt{2\pi}}{\upsilon h K_I\delta_y}, \quad (15)$$

where, h, E, υ, λ and δ_y are known parameters. For instance, the final polar relation for dark fringes for case 6 is reduced to:

$$r=\left[\frac{6.6369}{N_y}\sin\frac{3\theta}{2}\right]^{\frac{2}{3}}, \quad (16)$$

where, r is in mm (the plot is displayed in Fig. 6).

5. Numerical Simulation

Another practical simulating aid is FEM. In most of the well known finite element software direct evaluation of $\partial w/\partial x$ or $\partial w/\partial y$ is not possible. To achieve that, calculation of first partial derivatives of out-of-plane displacement needs to be post programmed and then calculated. Since the problem considered is symmetric with respect to x- axis and midplane of the model, it is sufficient to model ¼ of the sample. The symmetry is taken into account by blocking the corresponding degrees of freedom. Since the derivatives of the out-of-plane displacement component are sought, 20-node solid elements having midside nodes are used. For instance in case 6, the tensile load is modeled as a negative edge pressure of 2.998 MPa. First derivative

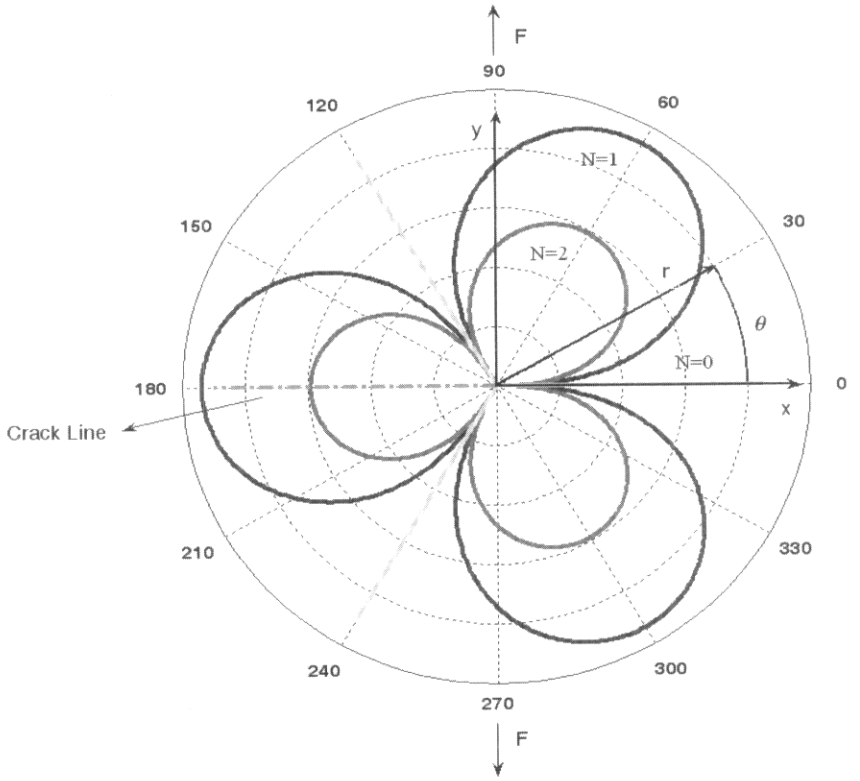

Fig. 6. Analytically simulated shearographic fringes for case 6.

contours at the vicinity of the crack tip are displayed as different colors (or grey levels) (Fig. 7). From one color to the next (or one grey level to the next) the slop changes by 0.0001.

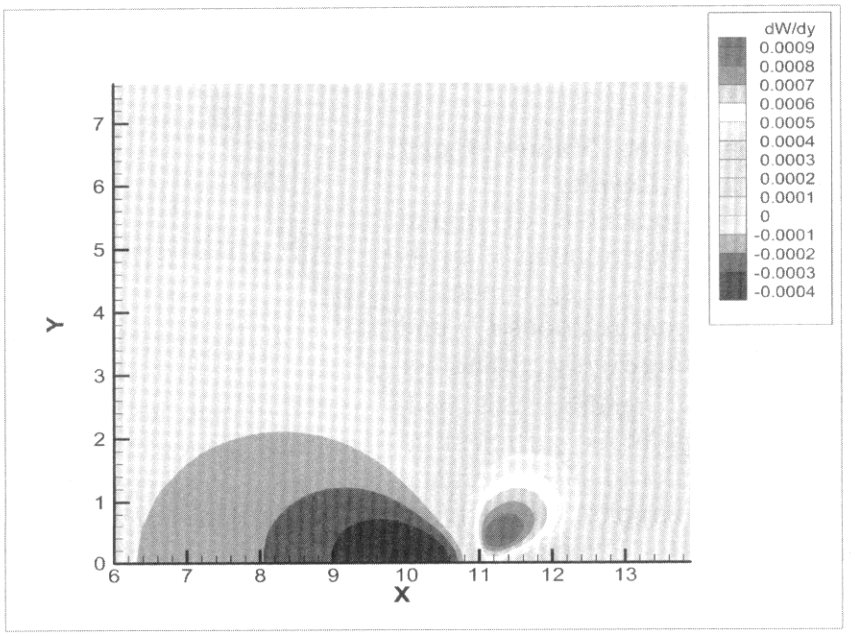

Fig. 7. Contours of $\partial w/\partial y$ at the vicinity of the crack tip for typical case 6.

Three elements have been used along thickness and total number of elements and nodes amount to 8097 and 41229, respectively. It is worth noting that since calculation of stress intensity factor is not intended in FEM modeling, singular elements are not used.

By comparison, FEM simulated fringes are in good agreement with those simulated analytically (configuration of fringes in Figs. 6,7), except at the origin where r becomes zero. That's because in the denominator of right hand side of Eq. (16), r takes positive values greater than zero and thus Eq. (16) does not hold true wherever r becomes zero. But experimental results show some deviations from simulated results, although the generality of fringe shapes are approved. The reasons for deviations are briefed as follows.

In Eq.(8), only first terms of stress series are included and higher order terms are eliminated which is a source of deviation. Also during the tests, it was impossible to make illuminating direction exactly normal to the object surface and it made an angle of about 8° with the normal to the object. Besides, the crack was made with a 0.25 mm thick blade which created a blunt tip instead of a sharp tip.

6. Determination of K_I Values Using Digital Shearography Results

In this section the potential of digital shearography in determining stress intensity factors of cracked specimens is examined. By combining relations (7) and (13) and eliminating $\partial w/\partial y$, another relation for K_I is readily obtained. Although one data point is sufficient to determine K_I but in order to take advantage of whole field shearography and increase the accuracy, the data for several points are registered and least squares method is utilized. Thus the least squares function F is defined as:

$$F=\sum_{i=1}^{m}\left(\frac{\upsilon h K_I r_i^{\frac{-3}{2}}}{2E\sqrt{2\pi}}\sin\frac{3\theta_i}{2}-\frac{N_i\lambda}{2\delta_y}\right)^2, \qquad (17)$$

where m is the total number of data points. To minimize the error in determination of K_I, F is partially differentiated with respect to K_I and set equal to zero and thus, we have:

$$\frac{\partial F}{\partial K_I}=\sum_{i=1}^{m}\frac{\upsilon h K_I r_i^{-3}}{2E\pi}\sin^2\frac{3\theta_i}{2}-\sum_{i=1}^{m}\frac{\lambda r_i^{\frac{-3}{2}}N_i}{\delta_y\sqrt{2\pi}}\sin\frac{3\theta_i}{2}. \qquad (18)$$

Then, K_I is readily obtained as:

$$K_I=\frac{\lambda E\sqrt{2\pi}}{\upsilon h\delta_y}\frac{\sum_{i=1}^{m}r_i^{\frac{-3}{2}}N_i\sin\frac{3\theta_i}{2}}{\sum_{i=1}^{m}r_i^{-3}\sin^2\frac{3\theta_i}{2}}. \qquad (19)$$

Using this approach, the SIF values are obtained for six test cases as given in Table 3. These SIF values are compared against those obtained through empirical relations. For instance, according to [15] the following relations yield first mode SIF for edge cracked specimens with finite dimensions under opening mode loading:

$$K_I=Y\sigma\sqrt{\pi a}, \qquad (20)$$

where,

$$Y=1.122-0.231\left(\frac{a}{W}\right)+10.55\left(\frac{a}{W}\right)^2 -21.71\left(\frac{a}{W}\right)^3+30.382\left(\frac{a}{W}\right)^4 \qquad (21)$$

It should be noted that since dark fringes are somewhat thick, the data points are read from centerline of dark fringes. Also the data points too close to the crack tip produce higher errors which must be crossed out.

Table 3. Comparison of empirical and digital shearography SIFs.

Case	$K_{Shearography}$ (MPa $\sqrt{m}$)	$K_{empirical}$ (MPa $\sqrt{m}$) [17]	Error (%)
1	0.315	0.342	7.8
2	0.606	0.652	7
3	0.742	0.795	6.7
4	0.426	0.464	8.2
5	0.694	0.739	6.1
6	1.064	1.123	5.2

Although as the Table 3 indicates the accuracy of the approach, there are some differences due to a few error sources which follows: the distance between crack tip and data points is too small to measure accurately, and locating exact position of the crack tip on images is to some extent troublesome. Furthermore the dark bands of fringes are thick instead of narrow that are due to human eyes which cannot recognize where exactly the light intensity becomes minimum. Also the cracks were created by a 0.25 mm thick ring saw blade which creates blunt crack tips instead of sharp. In addition the illumination direction is not exactly normal to the object surface and makes an angle of about 8° with the viewing direction.

7. Conclusions

Comparing experimental and simulated fringes, the credibility of generality of fringe shapes obtained for a cracked specimen by means of non-destructive technique of digital shearography is proved. Also comparing the K_I values obtained by means of digital shearography with the ones obtained from empirical relations, it can be concluded that the experimental results are quite accurate. Maximum percentage of error was 8.2%. Table 3 shows that the associated error for small loads is higher.

Acknowledgements

This research was supported by Research Council of University of Tehran under grant No. 8106027/1/02 which is gratefully acknowledged.

References

1. Habib, K. "Thermally Induced Deformations Measured by Shearography", J. Optics and Laser Technology, Vol. 37, No. 6, pp. 509-512, 2005.
2. Santos, F., Vaz, M.M., and Monteiro, J. "A New Set-up for Pulsed Digital Shearography Applied To Defect Detection In Composite Structures", J. Optics and Lasers in Eng. Vol. 42, No. 2, pp. 131-140, 2004.
3. Kim, K., Kang, K.S., Kang, Y.J., and Cheong, S.K. "Analysis of an Internal Crack of Pressure Pipeline Using ESPI and Shearography", J. Optics & Laser Technology, Vol. 35, No. 8, pp. 639-643, 2003.
4. Chau, F.S. and Zhou, J. "Direct Measurement of Curvature and Twist of Plates Using Digital Shearography", J. Optics and Lasers in Engineering, Vol. 39, No. 4, pp. 431-440, 2003.
5. Dilhaire, S., Jorez, S., Cornet, A., Patiño Lopez, L.D., and Claeys, W. "Measurement of the Thermomechanical Strain of Electronic Devices by Shearography", J. Microelectronics Reliability, Vol. 40, No. 8-10, pp. 1509-1514, 2000.
6. Steinchen, W., Yang, L.X., Kupfer, G., Mäckel, P., and Vössing, F. "Non-destructive Testing of Aerospace Composite Materials Using Digital

Shearography", J. Aerospace Engineering, Vol. 212, No. 1, pp. 21-30, 1998.
7. Steinchen, W., Yang, L.X., and Kupfer, G. "Digital Shearography for Nondestructive Testing and Vibration Analysis", Experimental Techniques, J. Experimental Mechanics, pp. 20-23, 1997.
8. Hung, Y.Y. and Long, KW. "Industrial Residual Stress Measurement by Large Shear Computerized Shearography", Proceedings of Industrial Conf. on Advanced Technology in Experimental Mechanics, wakayama, Japan, pp. 406-410, 1997.
9. Hung, Y.Y. "Application of Digital Shearography for Testing of Composite Structures", J. Composites, Part B 30, pp. 765-773, 1999.
10. Vest, C.M. "Holographic Interferometry, Opaque Objects: Measurement of Displacement and Deformation", John Wiley, New York, 1979.
11. Hung, Y.Y. "Digital Shearography Versus TV-Holography for Non-destructive Evaluation", Proc. of 27th Int. Symp. on Automotive Technology and Automation, Aachen, Germany, pp. 513-526, 1994.
12. Hung, Y.Y. "Shearography: A New Optical Method for Strain Measurement and Non-destructive Testing", Optical Eng., Vol. 21, No. 3, pp. 391-395, 1982.
13. Klumpp, P.A. "Simple Spatial Filtering for Shearograms", J. Optics and Laser Technology, Vol. 21, No. 2, pp. 105-111, 1989.
14. Steinchen, W., Yang, L.X., Schuth, M., and Kupfer, G. "Electronic Speckle Pattern Shearing Interferometry (ESPSI) and It's Applications", SPIE (Society of Photo-Optical Instrumentation Engineers), Vol. 2321, pp. 249-252, 1994.
15. Tada, H., Paris, P.C., and Irwin, G.R. "The Stress Analysis of Cracks Handbook", 3rd Ed., ASME Press, New York, 2000.